Journal of Agricultural Machinery

Homepage: https://jame.um.ac.ir

Research Article
Vol. 14, No. 1, Spring 2024, p. 49-67

A Finite Element Model of Soil-Stress Probe Interaction under a Moving Rigid Wheel

M. Naderi-Boldaji[1*], H. Azimi-Nejadian[2], M. Bahrami[1]

1- Department of Mechanical Engineering of Biosystems, Faculty of Agriculture, Shahrekord University, Shahrekord, Iran
2- Department of Mechanical Engineering of Biosystems, Faculty of Agriculture, Jahrom University, Jahrom, Iran
(*- Corresponding Authors Email: naderi.mojtaba@sku.ac.ir)

Received: 29 August 2023
Revised: 07 October 2023
Accepted: 09 October 2023
Available Online: 09 October 2023

How to cite this article:
Naderi-Boldaji, M., Azimi-Nejadian, H., & Bahrami, M. (2024). A Finite Element Model of Soil-Stress Probe Interaction under a Moving Rigid Wheel. *Journal of Agricultural Machinery, 14*(1), 49-67. https://doi.org/10.22067/jam.2023.84158.1185

Abstract

Machinery traffic is associated with the application of stress onto the soil surface and is the main reason for agricultural soil compaction. Currently, probes are used for studying the stress propagation in soil and measuring soil stress. However, because of the physical presence of a probe, the measured stress may differ from the actual stress, i.e. the stress induced in the soil under machinery traffic in the absence of a probe. Hence, we need to model the soil-stress probe interaction to study the difference in stress caused by the probe under varying loading geometries, loading time, depth, and soil properties to find correction factors for probe-measured stress. This study aims to simulate the soil-stress probe interaction under a moving rigid wheel using finite element method (FEM) to investigate the agreement between the simulated with-probe stress and the experimental measurements and to compare the resulting ratio of with/without probe stress with previous studies. The soil was modeled as an elastic-perfectly plastic material whose properties were calibrated with the simulation of cone penetration and wheel sinkage into the soil. The results showed an average 28% overestimation of FEM-simulated probe stress as compared to the experimental stress measured under the wheel loadings of 600 and 1,200 N. The average simulated ratio of with/without probe stress was found to be 1.22 for the two tests which is significantly smaller than that of plate sinkage loading (1.9). The simulation of wheel speed on soil stress showed a minor increase in stress. The stress over-estimation ratio (i.e. the ratio of with/without probe stress) noticeably increased with depth but increased slightly with speed for depths below 0.2 m.

Keywords: FEM simulation, Machinery traffic, Soil bin, Soil stress, Stress probe

Introduction

With the increase in the world's population, the need for food production has increased, which has led to more intense exploitation of the soil for more production. This was accompanied by an increase in the size and weight of farming machines to increase production capacity (Keller, Lamandé, Naderi-Boldaji, & de Lima, 2022). The increased weight of the machinery intensified soil degradation due to soil compaction. Soil compaction reduces the soil porosity, aeration, and water retention capacity and increases resistance to root penetration, surface runoff, soil erosion, and the energy required for tillage causing a series of effects that negatively affect crop yield and increase production costs (Hamza & Andersson, 2005; Nawaz, Bourrie, & Trolard, 2013; Shahgholi, Ghafouri Chiyaneh, & Mesri Gundoshmian, 2018).

It might be possible to prevent traffic-induced soil compaction by ensuring that the stress applied to the soil never exceeds the soil strength (Koolen & Kuipers, 1983). Conventionally, analytical methods based on

https://doi.org/10.22067/jam.2023.84158.1185

Boussinesq's theory of stress distribution (Boussinesq, 1885) have been used to predict soil stress propagation and the resulting compaction. Some of these models include SOCOMO (van den Akker, 2004), SoilFlex (Keller, Défossez, Weisskopf, Arvidsson, & Richard, 2007), Terranimo (Stettler *et al.*, 2014), and REPRO (Rücknagel *et al.*, 2015) all of which consider the soil as a continuum, elastic, homogeneous, and isotropic material. More accurate stress propagation models have been developed by including a stress concentration factor that varies with soil strength conditions (Frohlich, 1934; Söhne, 1953). Additionally, we need to measure the soil stress and validate the stress estimation calculated with the analytical models. Stress probes come in many shapes and forms. For example, fluid-inclusion probes i.e. Bolling probes (Bolling, 1985) or strain-gauged load cell transducers (Schjønning, Lamandé, Tøgersen, Arvidsson, & Keller, 2008; de Lima & Keller, 2021; Bahrami, Naderi-Boldaji, Ghanbarian, & Keller, 2023) cause the measured stress to deviate from the actual stress which occurs in the absence of the probe, while the actual stress causes soil compaction. The reasons for stress deviation can be the disturbance of the soil structure during the probe installation, the quality of the contact between the probe and the soil, the concentration of stress on the probe due to the arching effect, and the difference between the probe's stiffness and the stiffness of its surrounding soil (Kirby, 1999a, and 1999b). Therefore, the stress probe may under- or over-estimate the true soil stress. This difference is affected by the probe geometry, loading geometry, loading time, and mechanical properties of the soil (Weiler & Kulhawy, 1982). It is possible to correct the probe-measured stress to the soil's true stress by modeling the stress fields around the probe and finding a relationship for estimating the stress deviation due to embedding the probe into the soil.

Apart from analytical approaches, numerical simulation tools are widely applied for analyzing the stress propagation and soil compaction caused by machinery traffic. The main numerical methods used for simulation of stress propagation in soil can be categorized into finite element method (FEM), discrete elements method (DEM), and smoothed particle hydrodynamics (SPH). In FEM, considering the soil as a continuum medium using the theories of continuum mechanics, stress propagation is analyzed by calculating the stress on each element in contact with its adjacent element. In DEM, the stress transmission is analyzed by calculating the contact forces between the particles using Newton's second law, and the stress is transmitted through a chain of particles in contact with each other. In SPH, the particles are modeled in a fluid bed, and solving does not require meshing like the computational fluid dynamics method.

Several studies have used FEM to simulate stress propagation in the soil or the soil-tire interaction (e.g. Peth, Horn, Fazekas, & Richards, 2006; Cueto, Coronel, Bravo, Morfa, & Suárez, 2016; Keller, Ruiz, Stettler, & Berli, 2016; Silva *et al.*, 2018; Farhadi, Golmohammadi, Sharifi Malvajerdi, & Shahgholi, 2020; Jimenez *et al.*, 2021). Furthermore, the simulation of stress propagation in soil using DEM has been considered in multiple recent research studies (e.g. De Pue & Cornelis, 2019; De Pue, Lamandé, & Cornelis, 2020; Acquash & Chen, 2021; Bahrami, Naderi-Boldaji, Ghanbarian, & Keller, 2022; Bahrami *et al.*, 2023). However, we only found one recent study of modeling soil stress under tire traffic that used SPH (Gheshlaghi & Mardani, 2021). In most of the studies reported so far, either the propagation of soil true stress or the resulting soil compaction have been considered. However, the interaction between the soil and the stress probe and the difference between true and probe-measured stresses was studied less commonly. A recent study by de Lima and Keller (2021) investigated the probe stress deviation as affected by probe geometry (in terms of the ratio of diameter to height), difference in soil and probe material stiffness, and interference of multi-probe setups under

static loading using FEM. However, soil-probe interaction under dynamic loading (like a passing wheel) is an aspect that has been studied less frequently.

In a study conducted at Shahrekord University, Iran (Bahrami *et al.*, 2020, 2022, and 2023), Bahrami *et al.* (2022), the results of FEM and DEM for simulation of stress propagation under circular surface loading using plate sinkage test were compared. Stress was measured using a cylindrical load cell probe at 0.15 m depth in clay loam soil with 11% water content. The results showed that FEM may overestimate the probe-induced stress deviation due to the continuum nature of the soil in contact with the stress probe. The stress overestimation ratio (i.e. the ratio of with/without probe stress) was much larger in FEM than in DEM simulations. Consequently, Bahrami *et al.* (2023) investigated the interaction between soil and the stress probe under a moving rigid wheel in a soil bin for simulating the stress propagation in soil using DEM. The results showed that by modeling the soil with 10 mm diameter particles, the simulated stress with the probe was about 12% higher than the simulated true stress which was in close agreement with the results obtained from plate sinkage loading. The simulation of stress with varying wheel speed showed almost no significant effect. However, the results are still insufficient to acknowledge DEM as the best simulation approach for stress propagation for soils in different conditions. A freshly tilled or aggregated soil may be better simulated using DEM while a wet and compact soil may resemble more of a continuum nature which is better modeled using FEM. Whether using DEM or FEM, it is important to understand how the probe-induced stress deviation may vary under loading geometry, static *vs.* dynamic loading, depth, and loading time (speed).

The present study aims to simulate the stress propagation under the rigid wheel tested in a soil bin and the interaction between the soil and a stress probe using FEM to see how the stress overestimation ratio under wheel loading may differ from that of under plate sinkage loading, both simulated using FEM. It was hypothesized that the stress overestimation ratio obtained using FEM is not influenced by loading geometry, depth, and loading time (speed). Therefore, the objectives of this study are to (i) develop a FEM model of soil-probe interaction to study the stress propagation in soil under a rigid wheel and compare the simulated and measured stress, (ii) simulate the effect of wheel speed on soil stress and wheel sinkage, and (iii) evaluate the stress overestimation ratio under the moving wheel with various depths, wheel speeds, and probe geometries. The experimental data of two-wheeling tests conducted in a soil bin by Bahrami *et al.* (2023) were used for comparison with the FEM model predictions.

Materials and Methods

FEM model of soil-stress probe interaction under a moving rigid wheel

The FEM model of soil-wheel-stress probe interaction was developed in ABAQUS/CAE (Dassault Systemes Simulia Corp., Providence, RI, USA). According to the geometry and the symmetry of the model, a half-model with a plane of symmetry was generated. In this model, the soil was defined as a deformable material, and the wheel and the stress probe were modeled as rigid bodies. A wheel with a diameter of 0.27 m and a width of 0.15 m was modeled similar to the wheel used for the experimental tests in the soil bin. The stress probe was modeled in the form of a cylindrical probe consisting of two parts; the force-sensing surface (sensor) with 0.05 m diameter and the housing that is 0.07 m in diameter and 0.03 m in height (Bahrami *et al.*, 2022, and 2023). This allowed to evaluate the effect of the ratio of housing to sensor diameter on the stress overestimation ratio under loading of the moving wheel. To assemble the probe into the soil at a given depth and define the contact surfaces, a similar cylinder was cut from the soil where the probe is placed. Then, the probe is placed in the soil with an axisymmetric movement constraint.

The soil box was generated with dimensions of 2 × 1 × 1 m (length × width ×

depth). The model parts were assembled so that the wheel was placed on the soil surface and the stress probe into the soil at 0.15 m depth (Fig. 1a). The model's output is the force applied to the sensor surface during the movement of the wheel. Probe stress was calculated by dividing the force by the area of the probe sensing surface. The dependency of the FEM solution on mesh density was evaluated to select the appropriate size of the soil elements. For this purpose, six models were created with element sizes of 30, 25, 20, 15, 10, and 5 mm. In all simulations, the wheel speed was set at 1 m s^{-1} with 1,200 N vertical loading on the wheel axle. The true stress (i.e. the element vertical stress) at 0.15 soil depth was plotted against the element size for an elastic soil with 2 MPa elastic modulus and 0.3 Poisson's ratio. The stress increased sharply with elements larger than 10 mm (not shown). The stress difference in the simulations with 5 and 10 mm elements was less than 1%. Therefore, the element size of 10 mm was selected for the following simulations (Fig. 1b). The wheel-soil and stress probe-soil contacts were defined by the surface-to-surface contact method, and the value of the friction coefficient between the surfaces was assumed to be 0.5 (Ucgul, Saunders, & Fielke, 2017). The boundary conditions for the soil box and wheel were defined. The wheel was constrained to rotate and move the distance along the soil bin's length at varying speeds i.e. varying the traveling time. The wheel was free to move in the vertical direction and to sink into the soil. The wheel was free-rolling with no input torque. With-probe and without-probe stresses were analyzed under the moving wheel for each simulation. To measure the without-probe stress, the vertical stress of the soil element at a given depth was obtained from the model. For every simulation, the with-probe stress was higher than the without-probe stress which is due to the stress concentration around the probe owing to the arching effect. The arching effect occurs on the contact surface between two objects due to the difference between the yield strengths of the materials (Labuz & Theroux, 2005). The ratio of with-probe to without-probe stress was calculated as the stress overestimation ratio.

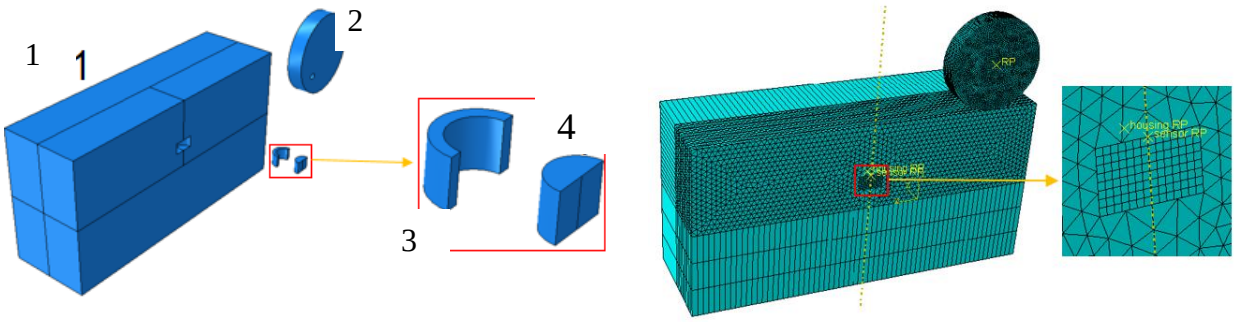

(a) (b)

Fig.1. (a) FEM model parts, 1- Soil box, 2- Rigid wheel, 3- Stress probe housing, 4- Probe sensing surface, and (b) Finite element mesh of the assembled model

In this study, soil was defined either as a pure-elastic or as an elastic-perfectly plastic material with a linear Drucker-Prager yield criterion. Drucker-Prager yield criterion has been used in many studies in the field of soil-machine interaction (Xia, 2011; Azimi-Nejadian, Karparvarfard, Naderi-Boldaji, & Rahmanian-Koushkaki, 2019; Arefi, Karparvarfard, Azimi-Nejadian, & Naderi-Boldaji, 2022; Mahboub & Mardani 2022; Naderi-Boldaji, Karparvarfard, & Azimi-Nejadian, 2023). It is necessary to define the modulus of elasticity and Poisson's ratio for elastic properties, and Drucker-Prager's internal angle of friction (β) and compressive yield stress for plastic properties. Drager-Prager friction angle can be calculated using the Mohr-Coulomb friction angle (φ) obtained

from the direct shear test (ABAQUS, 2019) defined in Eq. 1.

$$\beta = \frac{6 \sin \varphi}{3 - \sin \varphi} \quad (1)$$

The compressive yield stress (σ_c) is theoretically related to soil cohesion (c) and is given in Eq. 2.

$$\sigma_c = 2c \frac{cos\ \varphi}{1 - sin\ \varphi} \quad (2)$$

The compressive yield stress is an important parameter in determining the soil strength and analyzing the soil compressibility behavior (Khalid, Farooq, & Mujtaba, 2018). Considering the soil's elastic-perfectly plastic behavior allows us to define a distinct border between elastic and plastic deformations by defining the compressive yield stress.

Stress propagation as affected by soil elastic-plastic properties

A series of simulations were performed to evaluate the soil's true stress with changes in soil elastic-plastic properties (i.e. the model input parameters). This helps to identify the most important soil parameters affecting the stress propagation and can be used for calibrating more accurately. For this purpose, each of the model's input parameters was examined in the range shown in Table 1. Simulations were carried out for both pure-elastic soil (with varying modulus of elasticity and Poisson's ratio) and elastic-plastic soil (with varying elastic and plastic parameters). The simulations were performed with a wheel loading of 1,200 N which, as explained later, is the condition of the experimental test II.

Table 1- The range of parameters tested in sensitivity analyses.

Soil behavior	Parameter	Tested range	References
Elastic	Young's modulus of elasticity (kPa)	10,000-200,000	Naderi-Boldaji *et al.* (2013); Azimi-Nejadian *et al.* (2019)
Elastic, Elastic-plastic	Poisson's ratio	0.1-0.4	
Elastic-plastic	Compressive yield stress (kPa)	20-200	
Elastic-plastic	Young's modulus of elasticity (kPa)	1,000-10,000	
Elastic-plastic	Coefficient of soil wheel friction	0.1-0.5	
Elastic-plastic	Internal angle of friction (°)	10-50	

Experimental data of vertical stress under the moving wheel

The experimental stress data measured under a Teflon wheel for two soil conditions in a soil bin by Bahrami *et al.* (2023) were used as a reference for validating the modeling results. Fig. 2 shows a schematic of the soil bin equipped with a single testing wheel and its components. The soil bin is a 6 m long, 1 m wide, and 1 m deep soil box filled with clay loam soil (36% sand, 30% silt, and 34% clay). There is a double-sided blade on the carrier for soil movement and preparation. The testing wheel is positioned at the front of the carrier with a mechanism that allows varying the vertical loading on the wheel axle using standard weights. Further information concerning the soil bin can be found in Bahrami *et al.* (2023). Two wheeling tests were carried out in the soil bin at 11% water content at two soil compaction levels. The soil compaction levels were prepared by rolling the soil layers while preparing the soil until bulk densities of 1,200 and 1,350 kg m^{-3} were achieved for tests I and II, respectively. Test I and test II were carried out with 600 and 1,200 N wheel loading, respectively. The wheel speed for the two tests was 0.2 m s^{-1}. Soil stress was measured with a cylindrical load cell probe at 0.15 m soil depth. For each test, the soil cone index was measured in three replicates to a depth of 0.2 m before the wheeling test. Additionally, the wheel sinkage was measured with an image processing technique (Bahrami *et al.*, 2023).

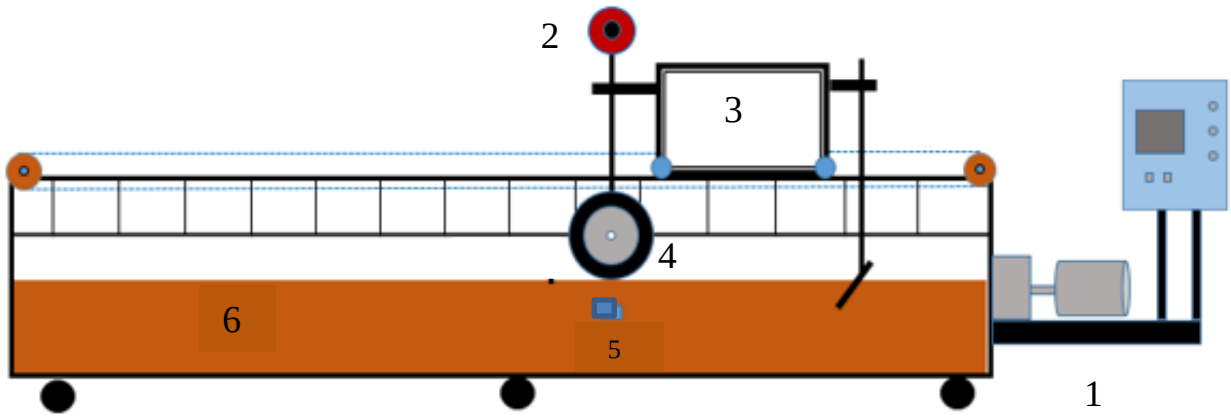

Fig.2. The schematics of the soil bin and wheel tester: 1- Drive system, 2- Weights applied to the wheel, 3- Carrier, 4- Testing wheel, 5- Load cell probe, and 6- Soil box (Bahrami *et al.*, 2023)

Calibration of the FEM input parameters

The elastic-plastic soil properties of the FEM model were calibrated using a similar approach as reported in Bahrami *et al.* (2023). Cone index and wheel sinkage into the soil were simulated and compared with the experimental results. The FEM model of cone penetration test developed by Naderi-Boldaji *et al.* (2023) was employed (Fig. 3). Naderi-Boldaji *et al.* (2023) showed the compressive yield strength and the angle of internal friction as the two parameters most affecting the soil's cone index. Hence, a simulation of the average cone index within 0-0.2 m depth was compared with the experimental cone index profile measured in the soil bin. Compressive yield strength was calibrated by matching the simulated and the experimental average cone indexes. Mohr-coulomb internal angle of friction was used by Bahrami *et al.* (2020) who measured the angle of friction for the same soil texture and water content using direct shear test. It was evaluated that the wheel sinkage into the soil is driven by the soil modulus of elasticity for a given vertical wheel loading. Matching the experimental and simulated wheel sinkage allowed the calibration of the soil's modulus of elasticity. We assumed a 0.3 value for Poisson's ratio as a routine assumption from previous studies (e.g. Ibrahmi, Bentaher, Hbaieb, Maalej, & Mouazen, 2015; Naderi-Boldaji, Hajian, Ghanbarian, & Bahrami, 2018). It was assumed that a minor difference between Poisson's ratio of the testing soil and the value assumed does not cause a significant error in prediction by the FEM model.

Table 2 gives the average values of elastic-plastic soil properties calibrated for the soil used for the two tests as well as the average experimental values for cone index and wheel sinkage. The average measured cone index values for tests I and II were 0.38 and 0.58 MPa, respectively, then the compressive yield stress values for these tests were calibrated as 75 and 90 kPa, respectively. The measured wheel sinkage for tests I and II were 30 and 15 mm, respectively. These values were obtained in the FEM simulation for the modulus of elasticity of 0.3 and 3 MPa, respectively. A decrease in the modulus of elasticity for each test increased the simulated wheel sinkage into the soil. For instance, by decreasing the modulus of elasticity from 1 to 0.1 MPa in test I, the wheel sinkage increased from 13.5 to 72.4 mm.

Finally, after calibrating the elastic-plastic parameters of the soil, stress simulation was performed for probe depths of 0.05, 0.1, 0.15, 0.2, 0.25, and 0.3 m with varying the wheel's speed in the range of 1-5 m s^{-1} to see how the soil stress and stress overestimation ratio are affected by probe depth and wheeling speed. Furthermore, the geometry of the stress probe was tested by varying the sensor diameter to

see the variations in stress overestimation ratio with the probe geometry.

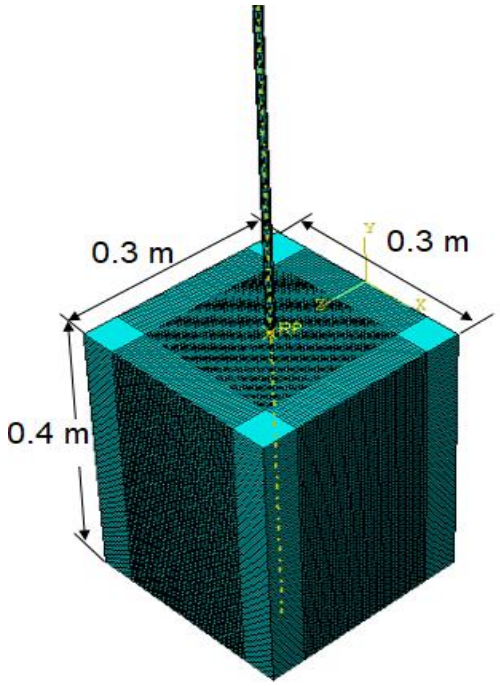

Fig.3. The FEM model of cone penetration test (Naderi-Boldaji *et al.*, 2023, Copyright 2023 by the International Society for Terrain-Vehicle Systems)

Table 2- The parameters measured in experimental tests and used for the FEM model calibration

Parameters	Test I	Test II
Measured soil density (kg m^{-3})	1,200	1,350
Measured coefficient of internal friction	0.24	0.24
Assumed Poisson's ratio	0.3	0.3
Wheel load (N)	600	1,200
Wheel speed (m s^{-1})	0.2	0.2
Measured wheel sinkage (mm)	30	15
Measured average cone index (MPa)	0.38	0.58
Calibrated Young's modulus (MPa)	0.3	3
Calibrated yield stress (kPa)	75	90

Results and Discussion

Stress propagation under the moving wheel

Figure 4a shows the simulation of the vertical stress propagation in soil under the moving wheel at a speed of 1 m s^{-1} with a wheel loading of 1,200 N. The stress bulb created under the wheel and the stress attenuation with depth can be seen. Stress transfer to the stress probe is observed when the wheel moves above the probe. A wheel rut was formed on the soil surface due to plastic deformation. The stress developed in the probe with the horizontal movement of the wheel is shown in Fig. 4b. A residual stress may be seen for elastic-plastic soils after the passing of the wheel which is attributed to the soil's plastic deformation. For pure-elastic soil, the soil's stress and deformation are expected to be fully recovered after the wheel passes.

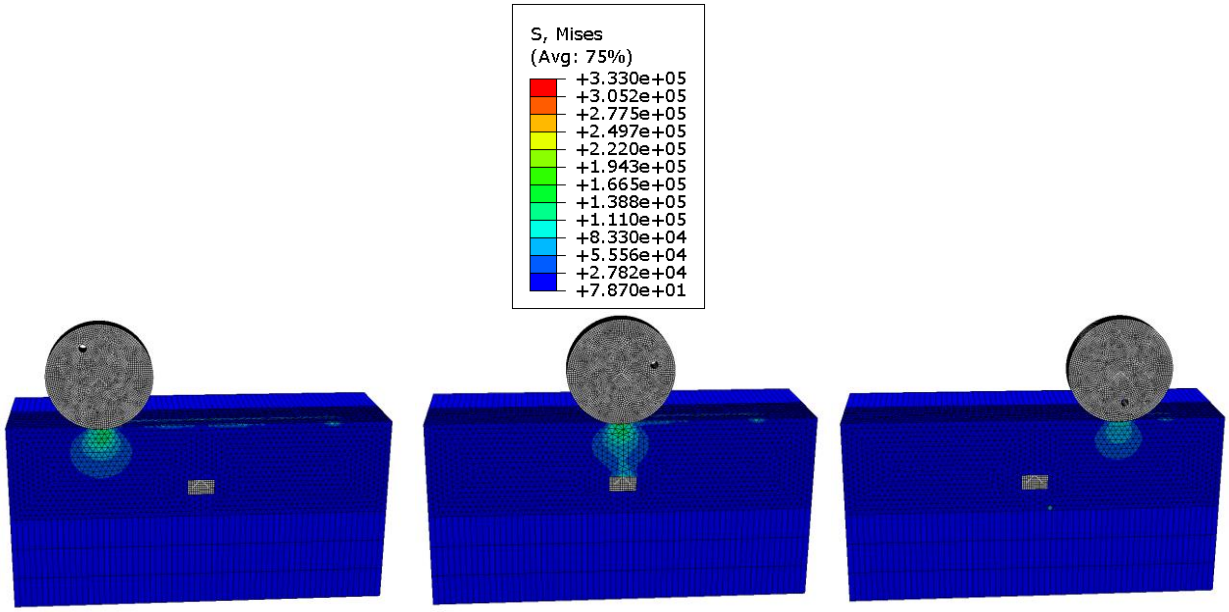

(a)

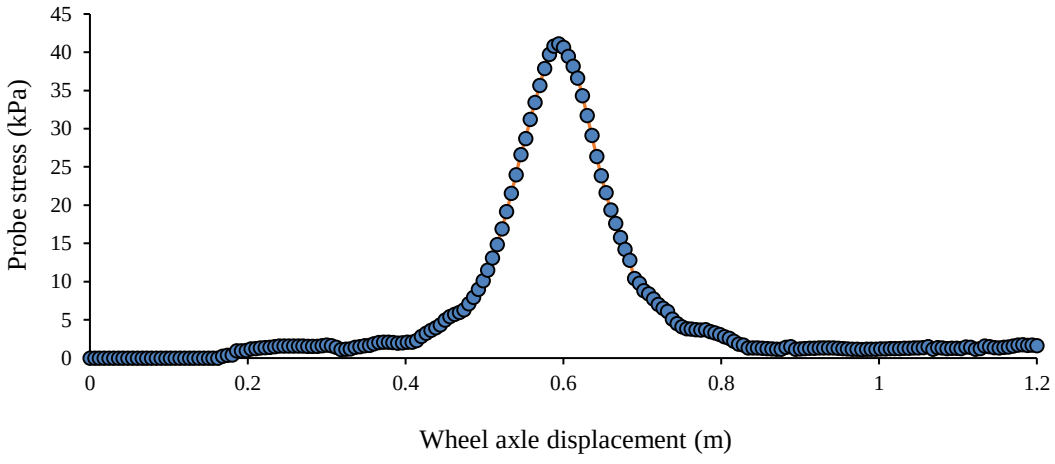

(b)

Fig.4. (a) Test II wheel movement simulation (the color bar legend indicates the Von Mises stress in soil), and (b) Variation in the simulated probe stress developed by wheel movement on the soil at a forward speed of 1 m s^{-1} and wheel loading of 1,200 N for Test II

Effect of soil elastic-plastic properties on soil stress

The results of analyses of the model parameters are first presented for pure-elastic soil (Fig. 5) and then for elastic-plastic soil (Fig. 6). As mentioned earlier, the true stress was analyzed for these analyses. For a pure-elastic soil, no effect of Young's modulus of elasticity and Poisson's ratio on soil stress was found under the wheel at a given loading (Fig. 5). This is in accordance with the analytical solution of vertical stress distribution using Boussinesq theory which is independent of soil properties.

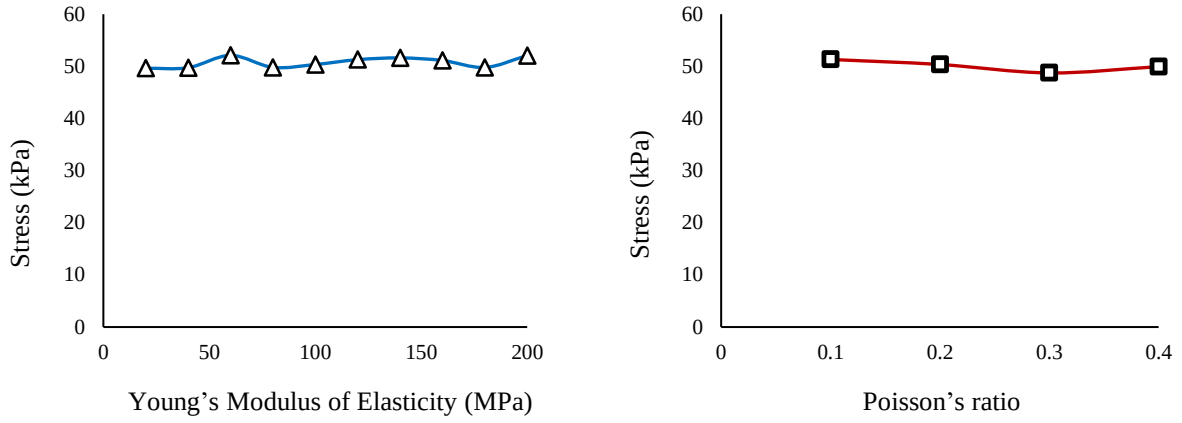

Fig.5. FEM-simulated peak true stress for a pure-elastic soil as functions of (a) Young's modulus of elasticity, and (b) Poisson's ratio at a wheel loading of 1,200 N

For the elastic-plastic soil, the stress in the soil noticeably changed with Young's modulus of elasticity (Fig. 6a) and the compressive yield stress (Fig. 6b). For ease of interpretation, the vertical axes of the plots shown in Fig. 6 are a normalized ratio of the stress simulated for the elastic-plastic soil to the corresponding stress for the pure-elastic soil, titled the stress concentration ratio. This ratio increased by increasing Young's modulus of elasticity to 6 MPa, and then decreased slightly with a further increase in the modulus of elasticity (Fig. 6a). This may be explained by the decrease in wheel sinkage into the soil and soil-wheel contact area which increases the ground normal stress at the soil-wheel interface.

With increasing the compressive yield stress, the stress concentration ratio approaches one, corresponding to a pure-elastic soil (Fig. 6b). The larger the stress concentration ratio, the higher the soil's plastic strain. At a given wheel loading, a higher plastic strain is obtained for smaller values of compressive yield stress. Soil with lower compressive strength could correspond to soil with a higher water content. For such soils, the stress concentration ratio is larger which confirms the interpretation of the stress concentration factor introduced by Frohlich (1934).

With increasing the soil-wheel coefficient of friction, the stress concentration ratio decreased slightly (Fig. 6c). This may be explained by the tangential frictional shear stresses created on the wheel-soil interface whose vertical stress components balance a portion of the wheel's load.

The stress concentration ratio decreased with increasing the internal angle of friction (Fig. 6d). With a particulate view of the soil media, larger friction between the particles attenuates the vertical stress with depth (Bahrami *et al.*, 2023). Although the Poisson's ratio had no effect on stress for pure-elastic soil, a slight increase in stress concentration ratio with increasing the Poisson's ratio was observed for elastic-plastic soil (Fig. 6e). This may be attributed to variations in the arching effect and the stress distribution on the probe's surface as affected by Poisson's ratio.

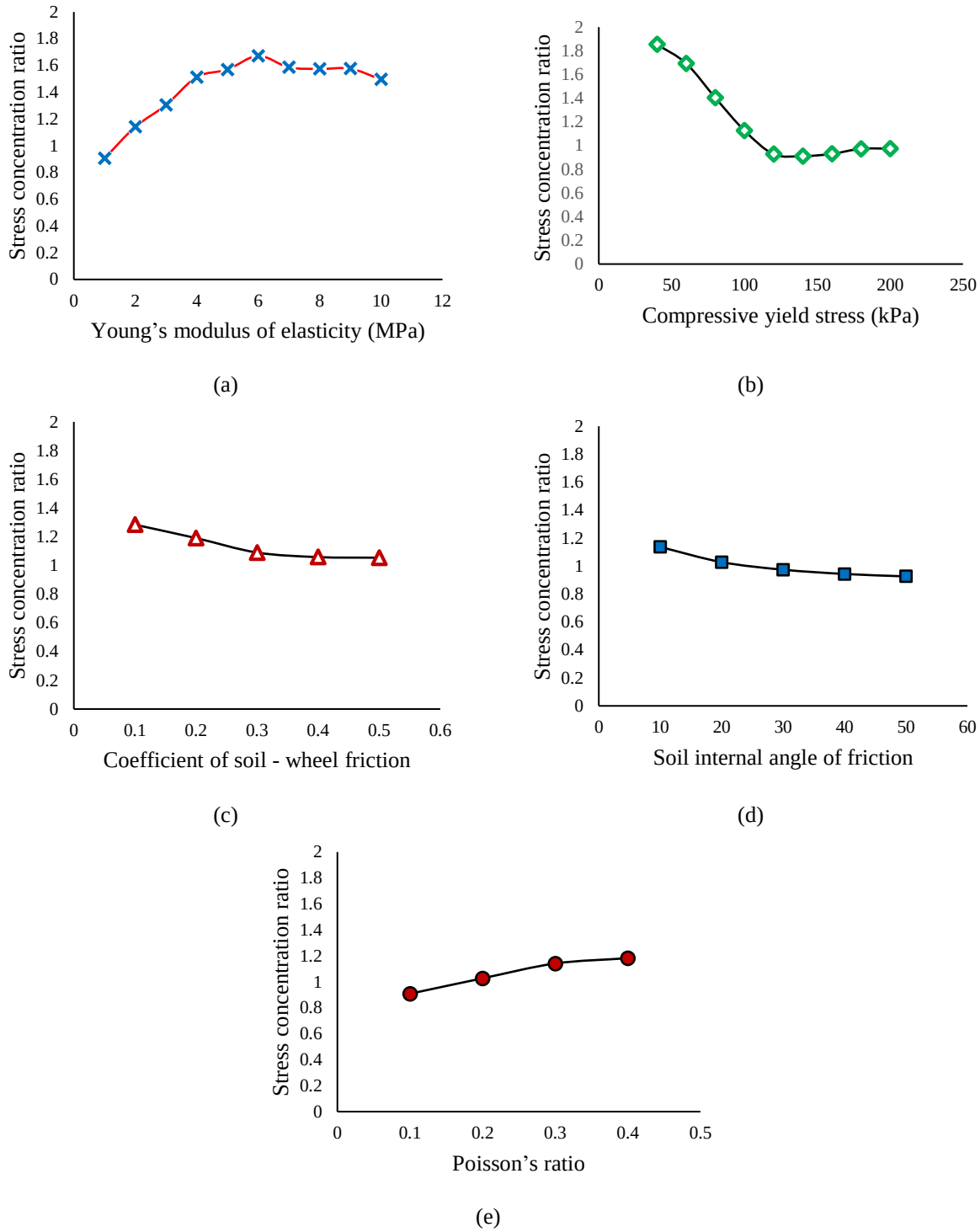

Fig.6. Stress concentration ratio, i.e. the ratio of simulated true stress of an elastic-plastic soil to the corresponding stress for a pure-elastic soil as functions of (a) Young's modulus of elasticity, (b) Compressive yield stress, (c) Coefficient of soil-wheel friction, (d) Soil internal angle of friction, and (e) Poisson's ratio.

Comparison of experimental and FEM-simulated stress

The FEM-simulated peak stress (with probe and without probe) as well as the

experimentally measured stress at the 0.15 m depth for test I (with bulk density of 1,200 kg m^{-3}) and test II (with bulk density of 1,350 kg m^{-3}) is shown in Fig. 7a and 7b, respectively. The peak stress measured under the wheel for test I and test II are 18 and 30 kPa, respectively. The larger value of stress for test II is due to the higher wheel loading. The FEM-simulated with-probe stress is larger than the experimental stress by 26.8% and 20.5% for tests I and II, respectively. The stress overestimation ratio (i.e. the ratio of simulated with-probe/without-probe stress) was found to be 1.27 and 1.17 for tests I and II, respectively. The difference in the stress overestimation ratio for test I and test II may be due to variations in the mechanical properties and plastic deformation of the soil (de Lima & Keller, 2021). The average overestimation ratio resulted here (1.22) is 0.1 larger than the DEM simulation results reported by Bahrami *et al.* (2023). However, the stress overestimation ratio is much smaller than the value obtained under FEM-simulated plate sinkage loading which was 1.9 (Bahrami *et al.*, 2022). This may be owing to the different boundary conditions or dynamic *vs.* static loading for the wheeling test and plate sinkage test, respectively.

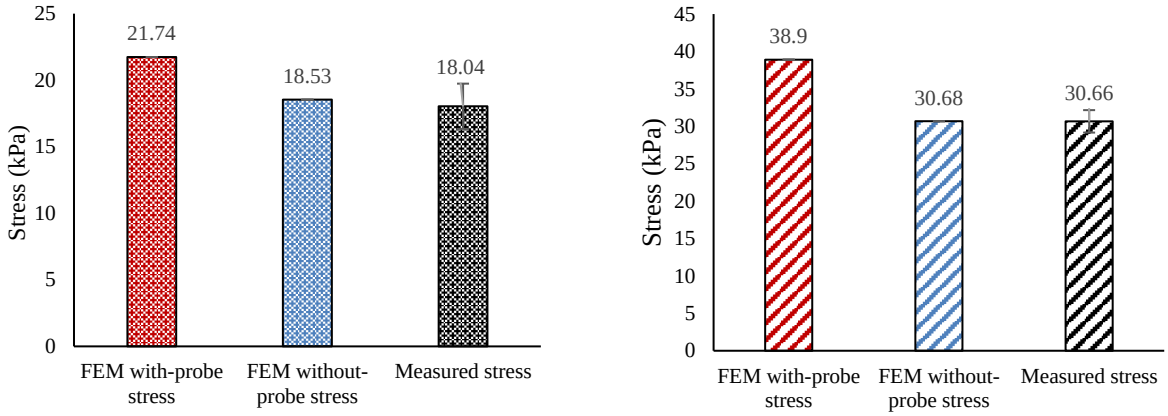

(a) (b)

Fig.7. Comparison of simulated and measured peak vertical stress for (a) test I (bulk density 12,00 kg m^{-3} and wheel loading of 600 N), and (b) test II (bulk density 1,350 kg m^{-3} and wheel loading of 1,200 N). The error bar in the measured stress column shows the standard error of replications (Bahrami *et al.*, 2023).

Stress overestimation ratio as affected by wheel speed and probe depth

Fig. 8 shows the simulated without-probe (Fig. 8a) and with-probe (Fig. 8b) stress as a function of wheel speed and depth for soil properties and wheel loading of test II. As expected, stress attenuates strongly with depth. Minor increases in without-probe stress can be seen with increasing wheel speed for any depth. However, with-probe stress slightly increases with wheel speed for depths higher than 0.15 m. For instance, at 0.3 m depth, increasing wheel speed from 1 to 5 m s^{-1} resulted in increased without-probe stress from 14.9 to 17.8 kPa and with-probe stress from 29.9 to 45.8 kPa which indicates a stronger effect of speed on with-probe stress. The slight increase in soil stress with the increased wheel speed can be explained by inertial effects. The stress overestimation ratio was plotted as a function of depth and wheel speed as shown in Fig. 9. It can be seen that, with the increasing speed of the wheel, the stress overestimation ratio at 0.3 m depth has increased to values larger than 2. The increase in stress overestimation ratio with increasing wheel speed is evident only at 0.25 and 0.3 m depths.

The results of previous literature on the

effect of traffic speed on soil stress are discrepant and almost contrasting. For instance, Naderi-Boldaji, Kazemzadeh, Hemmat, Rostami, and Keller (2018) reported that the average normal stress measured by the Bolling probe increased with tractor forward speed. On the other hand, some studies have shown a decrease in effective soil stress with increasing wheel speed (Horn, Blackwell, & White, 1989; Pytka, 2013). The variations in the experimental results may be due to the effect of pore water pressure at different soil water contents (Horn *et al.*, 1989). The effect of speed on soil stress and soil deformation is further discussed in the following section.

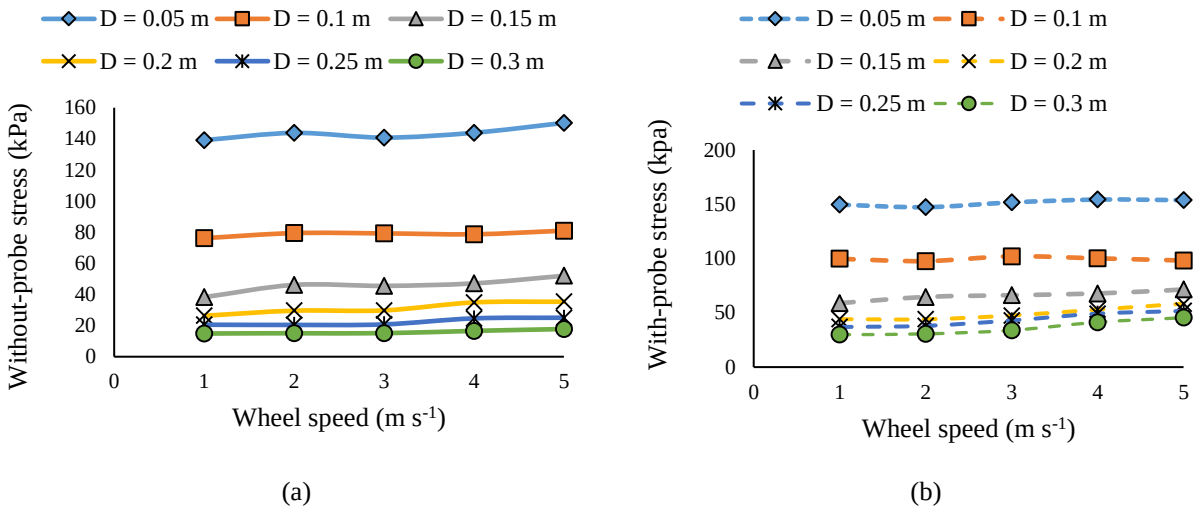

Fig.8. (a) Without-probe and (b) with-probe vertical stress as functions of wheel speed and depth for soil properties and wheel loading of test II at different probe depths

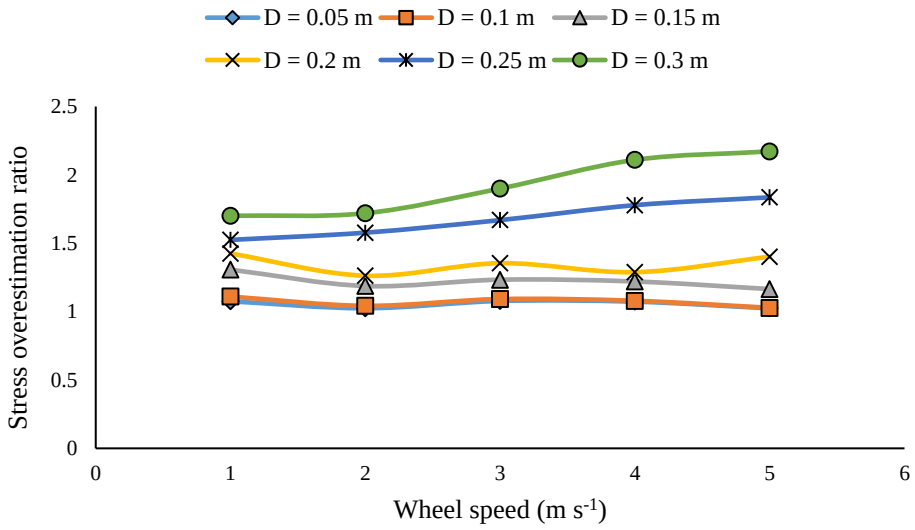

Fig.9. Stress overestimation ratio as a function of wheel speed at different probe depths

The effect of speed on wheel sinkage

Fig. 10 shows wheel sinkage as a function of wheel displacement and wheel speed for the soil properties and wheel loading of test II. Wheel sinkage increased rapidly once the wheel started moving and reached a constant value at the end of tests (Fig. 10a). The wheel speed had no significant effect on the wheel

sinkage, the average of which was calculated from wheel sinkage values of wheel displacement from 0.6 to 1 m (Fig. 10b). In this respect, the influence of forward speed on soil-wheel interaction performance such as wheel sinkage and wheel slippage was investigated by simulation. The results showed that the relative wheel sinkage decreased with forward speed (Shmulevich, Mussel, & Wolf, 1998). The effect of speed on soil compaction was investigated in field experiments by Stafford and de Carvalho Mattos (1981). In one research, the effects of forward speed, wheel load, and the number of passes on the soil density of a soil bin were investigated. Cone index and soil sinkage were considered indicators of soil compaction. The results showed the highest soil compaction occurred with the lowest wheel speed (Taghavifar & Mardani, 2014). They reported that the reason for the increase in soil compaction at low speeds is the increase in the soil-wheel contact time.

A review of soil compaction studies by machinery traffic shows that increasing the speed (or decreasing the loading time) decreases the compaction effect. Simulation of soil as an elastic-plastic material in our simulations might be the reason why wheel sinkage did not vary with wheel speed. The viscous effect in the soil is the parameter that changes the soil deformation with varying loading times where a part of external energy is dissipated due to the viscous effect. Or and Ghezzehei (2002) developed a modified Hertzian contact model of paired particles including the viscous effect. Transient loading caused by tire traffic and increasing traffic speed showed an obvious decrease in soil deformation and an increase in contact stress. This suggests that the simulation of soil as a visco-elastoplastic material is a reasonable scenario for modeling the effect of traffic speed on soil stress and soil compaction as similarly concluded by Bahrami *et al.* (2023).

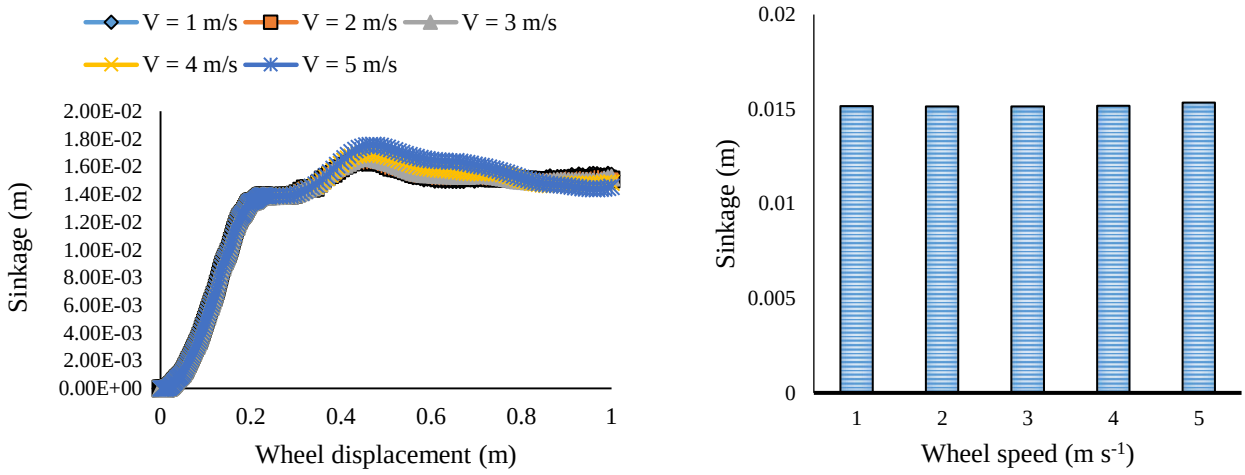

(a) (b)

Fig.10. (a) Simulated wheel sinkage as a function of wheel displacement, and (b) the average value of wheel sinkage between 0.6 and 1 m wheel displacement for different wheel speeds

Stress overestimation ratio and probe geometry

In a comparative study of the simulation of soil stress under plate sinkage loading using FEM and DEM, Bahrami *et al.* (2022) investigated the effect of probe geometry on the stress overestimation ratio. They found that the stress overestimation ratio decreased by increasing the ratio of housing diameter to sensor diameter. This suggested that a probe with a larger margin (i.e. the distance between the sensor and housing edge) has a smaller

stress concentration on the sensing surface of the probe. This is because the stress concentrates on the edge of the probe's housing. Hence, increasing the space between the probe housing edge and the sensing surface of the probe decreases the probe's stress reading. de Lima and Keller (2021) investigated the stress deviation of cylindrical probes as affected by probe design (material properties and probe height to diameter ratio), probe spacing in multi-probe setups, probe installation depth, and mechanical behavior of soil under static surface loading. However, the ratio of the probe housing diameter to the sensing's surface diameter was another factor first addressed by Bahrami *et al.* (2022) by modeling the stress probe in two pieces i.e. the probe housing and senor surface, installed under plate sinkage loading. A similar result was found under the moving wheel when the housing diameter was kept constant at 0.07 m and the sensor diameter was reduced from 0.06 m to 0.035 in 6 levels as shown in Fig. 11.

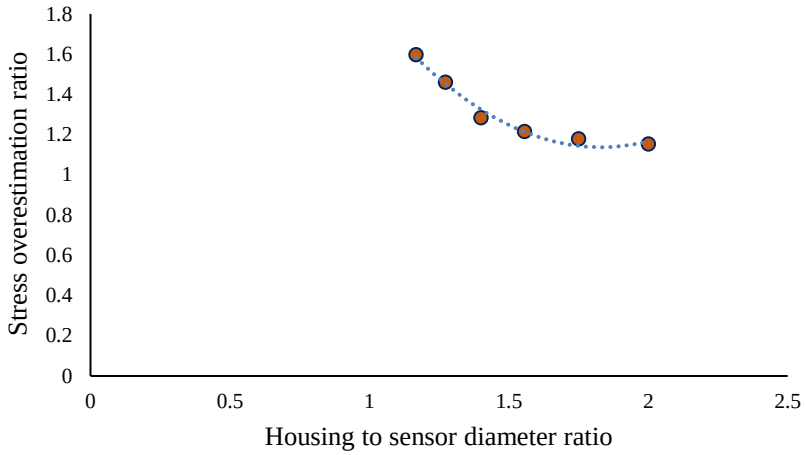

Fig.11. Stress overestimation ratio against housing to sensor diameter ratio

Conclusion

A finite element model of soil-stress probe interaction was developed to study the probe-induced stress deviation under a moving rigid wheel. Soil stress was analyzed in two conditions, with-probe stress, the stress measured or simulated with a cylindrical load cell probe, and without-probe, the soil's true stress simulated in the absence of the probe. The FEM-simulated with-probe stress was compared with the experimental stress measured in wheeling experiments in a soil bin. The following conclusions could be drawn:

1- Compared to the experimental stress, the model overestimated with-probe stress by 28.5%.
2- An average stress overestimation ratio, i.e. the ratio of simulated with-probe to without-probe stress, of 1.22 was found for the probe which is much smaller than that found under plate sinkage loading in a previous study. This was explained by the different boundary conditions and loading geometry of the wheel as compared to plate sinkage loading.
3- Wheeling speed had no noticeable effect on soil stress and stress overestimation ratio while stress overestimation ratio varied significantly with the probe's depth. Modeling the soil as an elastic-plastic material was discussed as the potential reason why soil stress and the resulting wheel sinkage did not vary with wheel speed. A minor increase in soil stress caused by increasing the speed might be due to inertial effects while the viscous effect is a more important aspect that needs further attention.

4- According to the results obtained under plate sinkage loading, increasing the ratio of the probe housing diameter to the sensor surface diameter decreased the stress overestimation ratio. This may suggest that, although the stress concentration is not only a function of probe geometry, the stress overestimation ratio could be minimized by optimizing the probe's design.
5- As compared to previous studies using DEM, a rather similar stress overestimation ratio was found under plate sinkage and wheel loading with DEM while the stress concentration ratio was significantly smaller under wheel loading than plate sinkage loading when modeled with FEM. This is likely explained by the continuum nature of FEM and the sponge effect on the soil surface which is strongly influenced by loading geometry.

Future studies could be aimed at studying soil stress propagation by parameterizing the soil as a visco-elastoplastic material to evaluate the effect of loading time on the resulting soil stress and deformation.

Acknowledgements

This study was conducted based on ideas from the third author's doctoral dissertation and the efforts of the second author who helped in FEM simulations. I, as the corresponding author, deeply regret that he (Dr. Hadi Azimi-Nejadian) passed away after the submission of this manuscript. I am sorry that we have lost an intelligent and hard-working scientist in the field of soil-machine interaction. God bless him.

References

1. ABAQUS, (2019). ABAQUS user's manuals version 6.19.1. Provid. RI ABAQUS, Inc. van den.
2. Acquah, K., & Chen, Y. (2021). Discrete element modeling of soil compaction of a press-wheel. *AgriEngineering*, *3*, 278-293. https://doi.org/10.3390/agriengineering3020019
3. Akker, J. J. (2004). SOCOMO: a soil compaction model to calculate soil stresses and the subsoil carrying capacity. *Soil and Tillage Research*, *79*, 113-127. https://doi.org/10.1016/j.still.2004.03.021
4. Arefi, M., Karparvarfard, S. H., Azimi-Nejadian, H., & Naderi-Boldaji, M. (2022). Draught force prediction from soil relative density and relative water content for a non-winged chisel blade using finite element modelling. *Journal of Terramechanics*, *100*, 73-80. https://doi.org/10.1016/j.jterra.2022.01.001
5. Azimi-Nejadian, H., Karparvarfard, S. H., Naderi-Boldaji, M., & Rahmanian-Koushkaki, H. (2019). Combined finite element and statistical models for predicting force components on a cylindrical mouldboard plough. *Biosystems Engineering*, *186*, 168-181. https://doi.org/10.1016/j.biosystemseng.2019.07.007
6. Bahrami, M., Naderi-Boldaji, M., Ghanbarian, D., & Keller, T. (2022). Simulation of soil stress under plate sinkage loading: A comparison of finite element and discrete element methods. *Soil and Tillage Research*, *223*, 105463. https://doi.org/10.1016/j.still.2022.105463
7. Bahrami, M., Naderi-Boldaji, M., Ghanbarian, D., & Keller, T. (2023). Discrete element modelling of stress propagation in soil under a rigid wheel in a soil bin: a simulation of probe inducing stress deviation and wheel speed. *Biosystems Engineering*, *230*, 159-170. https://doi.org/10.1016/j.biosystemseng.2023.04.013
8. Bolling, I. H. (1985). How to predict soil compaction from agricultural tires. *Journal of Terramechanics*, *22*(4), 205-223. https://doi.org/10.1016/0022-4898(85)90017-5
9. Boussinesq, M. J. (1885). Application Des Potentiels. Gauthier-Villars. https://books.google.com/books?id¼IYvpq89K_O8C
10. Cueto, O. G., Coronel, C. E. I., Bravo, E. L., Morfa, C. A. R., & Suárez, M. H. (2016). Modelling in FEM the soil pressures distribution caused by a tyre on a Rhodic Ferralsol

soil. *Journal of Terramechanics*, *63*, 61-67. https://doi.org/10.1016/j.jterra.2015.09.003
11. de Lima, R. P., & Keller, T. (2021). Soil stress measurement by load cell probes as influenced by probe design, probe position, and soil mechanical behavior. *Soil and Tillage Research*, *205*, 104796. https://doi.org/10.1016/j.still.2020.104796
12. De Pue, J., & Cornelis, W. M. (2019). DEM simulation of stress transmission under agricultural traffic Part 1: Comparison with continuum model and parametric study. *Soil and Tillage Research*, *195*, 104408. https://doi.org/10.1016/j.still.2019.104408
13. De Pue, J., Lamandé, M., & Cornelis, W. (2020). DEM simulation of stress transmission under agricultural traffic Part 2: Shear stress at the tyre-soil interface. *Soil and Tillage Research*, *203*, 104660. https://doi.org/10.1016/j.still.2020.104660
14. Farhadi, P., Golmohammadi, A., Sharifi Malvajerdi, A., & Shahgholi, G. (2020). Finite element modeling of the interaction of a treaded tire with clay-loam soil. *Computers and Electronics in Agriculture*, *162*, 793-806. https://doi.org/10.1016/j.compag.2019.05.031
15. Frohlich, O. K. (1934). Druckverteilung im Baugrunde. Springer Verlag, Wien, pp. 178
16. Gheshlaghi, F., & Mardani, A. (2021). Prediction of soil vertical stress under off-road tire using smoothed-particle hydrodynamics. *Journal of Terramechanics*, *95*, 7-14. https://doi.org/10.1016/j.jterra.2021.02.004
17. Hamza, M. A., & Anderson, W. K. (2005). Soil compaction in cropping systems: A review of the nature, causes and possible solutions. *Soil and Tillage Research*, *82*(2), 121-145. https://doi.org/10.1016/j.still.2004.08.009
18. Horn, R., Blackwell, P. S., & White, R. (1989). The effect of speed of wheeling on soil stresses, rut depth and soil physical properties in an ameliorated transitional red-brown earth. *Soil and Tillage Research*, *13*, 353e364. https://doi.org/10.1016/0167-1987(89)90043-3
19. Ibrahmi, A., Bentaher, H., Hbaieb, M., Maalej, A., & Mouazen, A. M. (2015). Study the effect of tool geometry and operational conditions on mouldboard plough forces and energy requirement: Part 1. Finite element simulation. *Computers and Electronics in Agriculture*, *117*, 258-267. https://doi.org/10.1016/j.compag.2015.08.006
20. Jimenez, K. J., Rolim, M. M., Gomes, I. F., de Lima, R. P., Berrío, L. L. A., & Ortiz, P. F. (2021). Numerical analysis applied to the study of soil stress and compaction due to mechanised sugarcane harvest. *Soil and Tillage Research*, *206*, 104847. https://doi.org/10.1016/j.still.2020.104847
21. Keller, T., Défossez, P., Weisskopf, P., Arvidsson, J., & Richard, G. (2007). SoilFlex: A model for prediction of soil stresses and soil compaction due to agricultural field traffic including a synthesis of analytical approaches. *Soil and Tillage Research*, *93*(2), 391-411. https://doi.org/10.1016/j.still.2006.05.012
22. Keller, T., Lamandé, M., Naderi-Boldaji, M., & de Lima, R. P. (2022). *Soil Compaction Due to Agricultural Field Traffic: An Overview of Current Knowledge and Techniques for Compaction Quantification and Mapping*. In: Saljnikov, E., Mueller, L., Lavrishchev, A., Eulenstein, F. (eds) Advances in Understanding Soil Degradation. Innovations in Landscape Research. Springer, Cham. https://doi.org/10.1007/978-3-030-85682-3_13
23. Keller, T., Ruiz, S., Stettler, M., & Berli, M. (2016). Determining soil stress beneath a tire: measurements and simulations. *Soil Science Society of America Journal*, *80*(3), 541-553. https://doi.org/10.2136/sssaj2015.07.0252
24. Khalid, U., Farooq, K., & Mujtaba, H. (2018). On yield stress of compacted clays. *International Journal of Geo-Engineering*, *9*(1), 1-16. https://doi.org/10.1186/s40703-018-0090-2
25. Kirby, J. M. (1999a). Soil stress measurement: Part I. Transducer in a uniform stress field. *Journal of Agricultural Engineering Research*, *72*(2), 151-160. https://doi.org/10.1006/jaer.1998.0357

26. Kirby, J. M. (1999b). Soil stress measurement. Part 2: transducer beneath a circular loaded area. *Journal of Agricultural Engineering Research*, *73*(2), 141-149. https://doi.org/10.1006/jaer.1998.0400
27. Koolen, A. J., & Kuipers, H. (1983). *Agricultural Soil Mechanics: Advanced Series in Agricultural Sciences* 13. Springer, Heidelberg, 241 pp. https://doi.org/10.1007/978-3-642-69010-5
28. Labuz, J. F., & Theroux, B. (2005). Laboratory calibration of earth pressure cells. *Geotechnical Testing Journal*, *28*(2), 188-196. https://doi.org/10.1520/GTJ12089
29. Mahboub Yangeje, H., & Mardani, A. (2022). Investigating the interaction between soil and cultivator blade by numerical simulation and validation of results by soil bin tests. *Journal of Agricultural Machinery*, *12*(4), 587-599. (in Persian with English abstract). https://doi.org/10.22067/jam.2021.70572.1041
30. Naderi-Boldaji, M., Alimardani, R., Hemmat, A., Sharifi, A., Keyhani, A., Tekeste, M. Z., & Keller, T. (2013). 3D finite element simulation of a single-tip horizontal penetrometer–soil interaction. Part I: Development of the model and evaluation of the model parameters. *Soil and Tillage Research*, *134*, 153-162. https://doi.org/10.1016/j.still.2013.08.002
31. Naderi-Boldaji, M., Kazemzadeh, A., Hemmat, A., Rostami, S., & Keller, T. (2018). Changes in soil stress during repeated wheeling: A comparison of measured and simulated values. *Soil Research*, *56*(2), 204-214. https://doi.org/10.1071/SR17093
32. Naderi-Boldaji, M., Hajian, A., Ghanbarian, D., & Bahrami, M. (2018). Finite element simulation of plate sinkage, confined and semi-confined compression tests: A comparison of the response to yield stress. *Soil and Tillage Research*, *179*, 63-70. https://doi.org/10.1016/j.still.2018.02.003
33. Naderi-Boldaji, M., Karparvarfard, S. H., & Azimi-Nejadian, H. (2023). Investigation of the predictability of mouldboard plough draught from soil mechanical strength (cone index *vs.* shear strength) using finite element modelling. *Journal of Terramechanics*, *108*, 21-31. https://doi.org/10.1016/j.jterra.2023.04.001
34. Nawaz, M. F., Bourrie, G., & Trolard, F. (2013). Soil compaction impact and modelling. A review. *Agronomy for sustainable development*, *33*, 291-309. https://doi.org/10.1007/s13593-011-0071-8
35. Or, D., & Ghezzehei, T. A. (2002). Modeling post-tillage soil structural dynamics: a review. *Soil and Tillage Research*, *64*(1-2), 41-59. https://doi.org/10.1016/S0167-1987(01)00256-2
36. Peth, S., Horn, R., Fazekas, O., & Richards, B. G. (2006). Heavy soil loading its consequence for soil structure, strength, deformation of arable soils. *Journal of Plant Nutrition and Soil Science*, *169*(6), 775-783. https://doi.org/10.1002/jpln.200620112
37. Pytka, J. A. (2013). *Dynamics of wheelesoil systems: A soil stress and deformation-based approach*. CRC Press, Taylor & Francis Group, LLC. https://doi.org/10.1201/b12729
38. Rücknagel, J., Hofmann, B., Deumelandt, P., Reinicke, F., Bauhardt, J., Hülsbergen, K. J., & Christen, O. (2015). Indicator based assessment of the soil compaction risk at arable sites using the model REPRO. *Ecological Indicators*, *52*, 341-352. https://doi.org/10.1016/j.ecolind.2014.12.022
39. Schjønning, P., Lamandé, M., Tøgersen, F. A., Arvidsson, J., & Keller, T. (2008). Modelling effects of tyre inflation pressure on the stress distribution near the soil–tyre interface. *Biosystems Engineering*, *99*(1), 119-133. https://doi.org/10.1016/j.biosystemseng.2007.08.005
40. Shahgholi, G., Ghafouri Chiyaneh, H., & Mesri Gundoshmian, T. (2018). Modeling of soil compaction beneath the tractor tire using multilayer perceptron neural networks. *Journal of Agricultural Machinery*, *8*(1), 105-118. (in Persian with English abstract).

https://doi.org/10.22067/jam.v8i1.58891
41. Shmulevich, I., Mussel, U., & Wolf, D. (1998). The effect of velocity on rigid wheel performance. *Journal of Terramechanics*, *35*(3), 189-207. https://doi.org/10.1016/S0022-4898(98)00022-6
42. Silva, R. P., Rolim, M. M., Gomes, I. F., Pedrosa, E. M., Tavares, U. E., & Santos, A. N. (2018). Numerical modeling of soil compaction in a sugarcane crop using the finite element method. *Soil and Tillage Research*, *181*, 1-10. https://doi.org/10.1016/j.still.2018.03.019
43. Söhne, W. (1953). Druckverteilung im Boden und Bodenformung unter Schlepperreifen (Pressure distribution in the soil and soil deformation under tractor tyres). *Grundl Land Technik*, *5*, 49-63. https://doi.org/10.1007/BF01512930
44. Stafford, J. V., & de Carvalho Mattos, P. (1981). The effect of forward speed on wheel-induced soil compaction: laboratory simulation and field experiments. *Journal of Agricultural Engineering Research*, *26*(4), 333-347. https://doi.org/10.1016/0021-8634(81)90075-5
45. Stettler, M., Keller, T., Weisskopf, P., Lamandé, M., Lassen, P., & Schjønning, P. (2014). Terranimo®–a web-based tool for evaluating soil compaction. *Landtechnik*, *69*(3), 132-138.
46. Taghavifar, H., & Mardani, A. (2014). Effect of velocity, wheel load and multipass on soil compaction. *Journal of the Saudi Society of Agricultural Sciences*, *13*(1), 57-66. https://doi.org/10.1016/j.jssas.2013.01.004
47. Ucgul, M., Saunders, C., & Fielke, J. M. (2017). Particle and geometry scaling of the hysteretic spring/linear cohesion contact model for discrete element modelling of soil-tool simulation. ASABE Paper No. 1701372. St. Joseph, MI: ASABE. https://doi.org/10.13031/aim.201701372
48. Van den Akker, J. J. H. (2004). SOCOMO: a soil compaction model to calculate soil stresses and the subsoil carrying capacity. *Soil and Tillage Research*, *79*(1), 113-127. https://doi.org/10.1016/j.still.2004.03.021
49. Weiler Jr, W. A., & Kulhawy, F. H. (1982). Factors affecting stress cell measurements in soil. *Journal of the Geotechnical Engineering Division*, *108*(12), 1529-1548. https://doi.org/10.1061/AJGEB6.0001393
50. Xia, K. (2011). Finite element modeling of tire/terrain interaction: Application to predicting soil compaction and tire mobility. *Journal of Terramechanics*, *48*(2), 113-123. https://doi.org/10.1016/j.jterra.2010.05.001

نشریه ماشین‌های کشاورزی
https://jame.um.ac.ir

مقاله پژوهشی

جلد ۱۴، شماره ۱، بهار ۱۴۰۳، ص ۶۷-۴۹

یک مدل اجزای محدود برهم‌کنش کاوشگر تنش-خاک زیر یک چرخ صلب متحرک

مجتبی نادری بلداجی[1*]، هادی عظیمی نژادیان[2]، مصطفی بهرامی[3]

تاریخ دریافت: ۱۴۰۲/۰۶/۰۷
تاریخ پذیرش: ۱۴۰۲/۰۷/۱۷

چکیده

تردد ماشین‌های کشاورزی با اعمال تنش بر سطح خاک دلیل اصلی تراکم خاک‌های کشاورزی است. مطالعه انتشار تنش در خاک نیاز به اندازه گیری تنش در خاک دارد، در حالی‌که تنش اندازه‌گیری‌شده با نصب هر نوع کاوشگر ممکن است با تنش واقعی خاک، یعنی تنش خاک در غیاب کاوشگر متفاوت باشد. این مطالعه با هدف شبیه‌سازی برهم‌کنش کاوشگر تنش در زیر یک چرخ صلب متحرک با استفاده از روش اجزای محدود به‌منظور بررسی تطابق تنش شبیه‌سازی‌شده با کاوشگر با تنش تجربی اندازه‌گیری‌شده در یک مخزن خاک انجام شد. خاک به‌عنوان یک ماده کشسان- خمیری مدل‌سازی و خواص آن با شبیه‌سازی نفوذ مخروط و نشست چرخ در خاک کالیبره شد. نتایج نشان داد که تنش به‌دست‌آمده از پروب با روش اجزای محدود به‌طور متوسط ۲۸ درصد بیش‌تخمینی در مقایسه با تنش تجربی برای بارهای چرخ ۶۰۰ و ۱۲۰۰ نیوتن داشته است. میانگین نسبت شبیه‌سازی‌شده تنش با کاوشگر به تنش بدون کاوشگر برای دو آزمون ۱/۲۲ به‌دست آمد که به‌طور معنی‌داری کوچک‌تر از همین نسبت تحت بارگذاری نشست صفحه دایره‌ای با مقدار ۱/۹ بود و همچنین به‌طور قابل‌توجهی بزرگ‌تر از نتیجه به‌به‌دست‌آمده از روش اجزای گسسته است. افزایش سرعت حرکت چرخ افزایشی جزئی در تنش خاک را نشان داد. نسبت بیش تخمینی تنش (همان نسبت تنش با کاوشگر به تنش بدون کاوشگر) به‌طور قابل‌توجهی با عمق افزایش یافت ولی افزایش کمی با سرعت در عمق زیر ۰/۲ متر داشت.

واژه‌های کلیدی: انباره خاک، تردد ماشین، تنش خاک، شبیه‌سازی اجزای محدود، کاوشگر تنش

۱- بخش مهندسی مکانیک بیوسیستم، دانشکده کشاورزی، دانشگاه شهرکرد، شهرکرد، ایران
۲- استادیار، بخش مهندسی مکانیک بیوسیستم، دانشکده کشاورزی، دانشگاه جهرم، جهرم، ایران
۳- دانش‌آموخته دکتری، بخش مهندسی مکانیک بیوسیستم، دانشکده کشاورزی، دانشگاه شهرکرد، شهرکرد، ایران
(*- نویسنده مسئول: Email: naderi.mojtaba@sku.ac.ir)

https://doi.org/10.22067/jam.2023.84158.1185